Analysis of the cohesion/adhesion proportion around bitumen-mineral failure interface under tensile loading

Shi, Baocun; Liu, Quan; Gao, Yangming; Wu, Jiantao; Chen, Jingya

DOI
10.1016/j.conbuildmat.2023.132555

Publication date
2023

Document Version
Final published version

Published in
Construction and Building Materials

Citation (APA)
Shi, B., Liu, Q., Gao, Y., Wu, J., & Chen, J. (2023). Analysis of the cohesion/adhesion proportion around bitumen-mineral failure interface under tensile loading. *Construction and Building Materials*, *399*, Article 132555. https://doi.org/10.1016/j.conbuildmat.2023.132555

Construction and Building Materials 399 (2023) 132555

Contents lists available at ScienceDirect

Construction and Building Materials

journal homepage: www.elsevier.com/locate/conbuildmat

Analysis of the cohesion/adhesion proportion around bitumen-mineral failure interface under tensile loading

Baocun Shi [a], Quan Liu [a,*], Yangming Gao [b], Jiantao Wu [a], Jingya Chen [a]

[a] College of Civil and Transportation Engineering, Hohai University, Nanjing 210098, Jiangsu, China
[b] Faculty of Civil Engineering and Geosciences, Delft University of Technology, 2628 CN Delft, Netherlands

ARTICLE INFO

Keywords:
Failure mode
Bitumen-aggregate interface
Adhesion/cohesion proportion
Mineral surface morphology
Film thickness

ABSTRACT

The occurrence of cohesive/adhesive hybrid failure at the bitumen-aggregate interface is widely acknowledged, however, the quantitative evaluation of the cohesion/adhesion proportion is relatively weak. This study explored cohesive/adhesive hybrid failure and provided a quantitative analysis of the proportion between cohesion and adhesion. For this reason, this study considered a variety of experimental factors that included temperature (5 °C, 15 °C, and 25 °C), mineral morphology (three mineral types and three surface textures), and measured film thickness (varying from 10 μm to 900 μm). By performing the bonding strength test, the strength was recorded and interface failure was accordingly captured. The results indicated that the cohesion/adhesion proportion varied significantly with the temperature, mineral morphology, and measured film thickness. In addition, it was found that bonding strength decreased with the increase in the film thickness and temperature, which can be well explained by variation in adhesion/cohesion proportion. Complete cohesive failure was observed when the film thickness increased beyond a critical value at a relatively high temperature. An additional noteworthy finding was the resemblance of a lunar crater for the failure interface at high temperatures, signifying the heterogeneous composition of the bituminous binder around the interface.

1. Introduction

The debonding of asphalt mixtures caused by moisture infiltration or vehicle loading is a long-term topic for pavement engineers [1,2]. In the past several decades, many efforts have been devoted to achieving a better understanding of the debonding mechanisms of asphalt mixtures. Representative theories include the weak boundary layer theory [3], mechanical adhesion theory [4], electrostatic theory [5], chemical bonding theory [6], and surface free energy theory [7]. Multiple experimental phenomena and a range of influencing factors were considered when creating these theories, and they effectively accounted for the bonding strength of the bitumen-aggregate interface in the face of external loads and moisture.

The accepted failure mode at the bitumen-aggregate interface is generally divided into cohesive, adhesive, and structural failure [8,9]. Nonetheless, either laboratory or in-field evidence indicated that the failure around the bitumen-aggregate interface normally occurred with a combination of adhesive and cohesive failure modes. Li et al. [10] investigated the influence of mineral filler on the bonding properties of bitumen mastics. As the increase in film thickness, the failure mode progressively switched from adhesive/cohesive failure to cohesive failure, indicating that the film thickness was a crucial factor of the bitumen-aggregate interface failure. Mishra et al. [11] investigated the influence of six different bitumen membrane thicknesses on the interfacial strength of basalt-unmodified bitumen systems. It was found that as the thickness of the bitumen membrane increased, the cohesive failure mode gradually became dominant, and the adhesion between bitumen and aggregate increased. Huang et al. [12] investigated the influence of experimental conditions and material properties on the adhesion performance of asphalt-aggregate interfaces. The results revealed that the interfacial failure strength of asphalt-aggregate exhibited a negative correlation with temperature and a positive correlation with pull-out rate. Additionally, short-term aging was found to enhance the bonding of the asphalt-aggregate interface, while long-term aging had the opposite effect. Bidgoli et al. [13] reported that adhesive and cohesive failure simultaneously occurred when the samples were subjected to moisture damage using the Lottman test. Accordingly, the adhesion-cohesion index was introduced to evaluate the moisture susceptibility of asphalt mixtures.

The use of the molecular dynamic method promoted the study of

* Corresponding author.
E-mail address: quan.liu@hhu.edu.cn (Q. Liu).

https://doi.org/10.1016/j.conbuildmat.2023.132555
Received 17 April 2023; Received in revised form 9 July 2023; Accepted 17 July 2023
Available online 22 July 2023

bitumen-aggregate interface failure at the nano-scale [14]. Gao et al. [15,16] evaluated the adhesive properties and debonding behavior of asphalt mixtures considering the mineral type and the presence of water and reported that the adhesive and debonding behavior were associated with the chemistry and mineralogical properties of the minerals. Chen et al. [17] simulated the pull-off test using the molecular dynamic method and found that the increase of film thickness induced the proportion of cohesion area from 29% to 65%. From the above, it can be concluded that the environmental temperature and experimental setup considerably affected the hybrid failure around bitumen-aggregate interface. Although some scholars theoretically or numerically identified the adhesive/cohesive hybrid failure mode, there is still a lack of quantitative identification for the hybrid failure mode and its influencing factors. For instance, Cala et al. [18,19] discussed the relationship between adhesive area applied maximum force or work of fracture, whereas the influence of measurement set up on the amount of adhesive area was not mentioned.

As indicated by the above literature review, the failure mode around the bitumen-aggregate interface has been well studied and understood by means of various approaches. However, there are a few studies particularly exploring the hybrid failure mode from a quantitative perspective. This study presents an experimental investigation of the adhesive/cohesive hybrid failure mode around the bitumen-aggregate interface in dry conditions from a quantitative perspective. In reality, moisture damage is normally the premise of the interface failure. Therefore, many studies considered moisture damage in their investigation of the bitumen-aggregate interface [20–22]. However, the purpose of this study aims to provide a quantitative analysis of the adhesion/cohesion proportion of the hybrid interface failure, particularly for its influencing factors. Therefore, moisture damage or wet conditions were not included in the experimental design for simplification. To this end, three mineral surfaces including basalt, limestone, and granite were used. In addition, the surface morphology was intendedly distinguished with varying polishing procedures. After the polishing, the surface free energy was characterized through the contact angle test. Subsequently, the Pneumatic Adhesion Tensile Strength Testing Instrument (PATTI) was adopted to measure the bonding strength between bitumen and aggregate surface at different temperatures, in which various film thicknesses were taken into account. Consequently, the adhesive/cohesive hybrid failure was analyzed through the digital image process.

2. Materials and experimental design

2.1. Bitumen and mineral surface

A kind of unmodified bitumen with a penetration grade of 60/80 was used in this study. The technical indicators were measured according to the specification JTG-E20-2011 (Ministry of Transport of the People's Republic of China 2011)[23], as shown in Table 1. All the test items satisfied the engineering requirement.

Three different mineral surfaces that included basalt, limestone, and granite, were considered in this study. The mineral surface was manufactured by cutting the mineral collected from the market into slabs with a dimension of 100 mm × 100 mm × 10 mm, as seen in Fig. 1.

Table 1
Technical indicators for used bitumen.

Bitumen	Test items	Measured values
Original bitumen	Penetration (25 °C, 100 g, 5 s)/0.1 mm	66
	Ductility (15 °C)/cm	>100
	Softening point/ °C	48.7
After aging (163 °C, 5 h)	Quality change/%	−0.2
	Residual penetration/%	63
	Residual ductility (10 °C)/cm	179

After several preliminary trials, the surface of mineral slabs was polished using a device combined with different sandpaper types and polishing times following the procedure shown in Table 2. In what follows, the structured light projection method was used to characterize the micro-texture of the mineral surface [24]. Based on the texture characterization, the mean texture depth (MTD) for each mineral surface can be accordingly calculated with the MATLAB code. Although the boundary area of the mineral surface was not polished uniformly as expected, the central areas can achieve a relatively good homogeneity state. As indicated in Fig. 1, the lateral bonding strength test and contact angle test were performed within the central areas. In this study, four parallel measurements were carried out for one slab, as shown in Fig. 1. Table 3 summarizes the combination of samples and test conditions in this study.

2.2. Control of film thickness between bitumen and mineral surface

This study aims to investigate the influence of film thickness on the interface failure mode. Before this, it is essential to precisely control the film thickness, in other words, featuring the correlation between film thickness and used bitumen mass. For this reason, this study utilized a film thickness gauge with a measurement range from 0 to 1250 μm with an accuracy of 0.1 μm to measure the film thickness of different bitumen masses. Considering that the gauge was invented for the measurement of coatings, it is not possible to directly measure the film thickness once the tensile head was adhered to the mineral surface. Alternatively, this study first used a plastic film with a known thickness of 160 μm to calibrate the film thickness of bitumen, as shown in Fig. 2. This experiment prepared 10 different bitumen thicknesses, namely 10, 100, 200, 300, 400, 500, 600, 700, 800, and 900 μm, to investigate their impact on the bitumen-mineral interface.

After preparing the bitumen-plastic interface with varying bitumen masses, the final bitumen film thickness can be obtained by deducting the thickness of the plastic film. In the end, the relationship between bitumen mass and the film thickness can be accordingly established, as shown in Table 4.

2.3. Experimental methods

2.3.1. Surface free energy of mineral slabs

The surface free energy of the mineral surface was measured by the contact angle instrument, as shown in Fig. 3. For each slab, four measurement positions corresponding to the bonding strength test were selected. Based on the literature [25,26], it was found that W-G-F (distilled water, glycerol, and formamide) is a widely used combination for the estimation of surface free energy components. Therefore, distilled water, glycerol, and formamide were used for the calibration of surface free energy. Following Eq. (1), the surface free energy can be calculated based on the measured contact angle. The interfacial adhesive energy bitumen and different aggregates were calculated by Eq. (2) [27].

$$\frac{\gamma_l(1+cos\theta)}{2}\frac{1}{\sqrt{\gamma_l^d}}=\sqrt{\gamma_s^p}\sqrt{\frac{\gamma_l^p}{\gamma_l^d}}+\sqrt{\gamma_s^d} \tag{1}$$

$$W_{adhension}=2\sqrt{\gamma_s^d\gamma_l^d}+2\sqrt{\gamma_s^p\gamma_l^p} \tag{2}$$

where γ_l refers to the surface free energy of the liquid; θ is the measured contact angle; $W_{adhension}$ is the adhesion energy; γ_s^d and γ_s^p are the dispersive and polar components of solid surface energy, respectively; γ_l^d and γ_l^p are the dispersive and polar components of liquid surface energy, respectively. Provided the standard liquids with known surface energies,

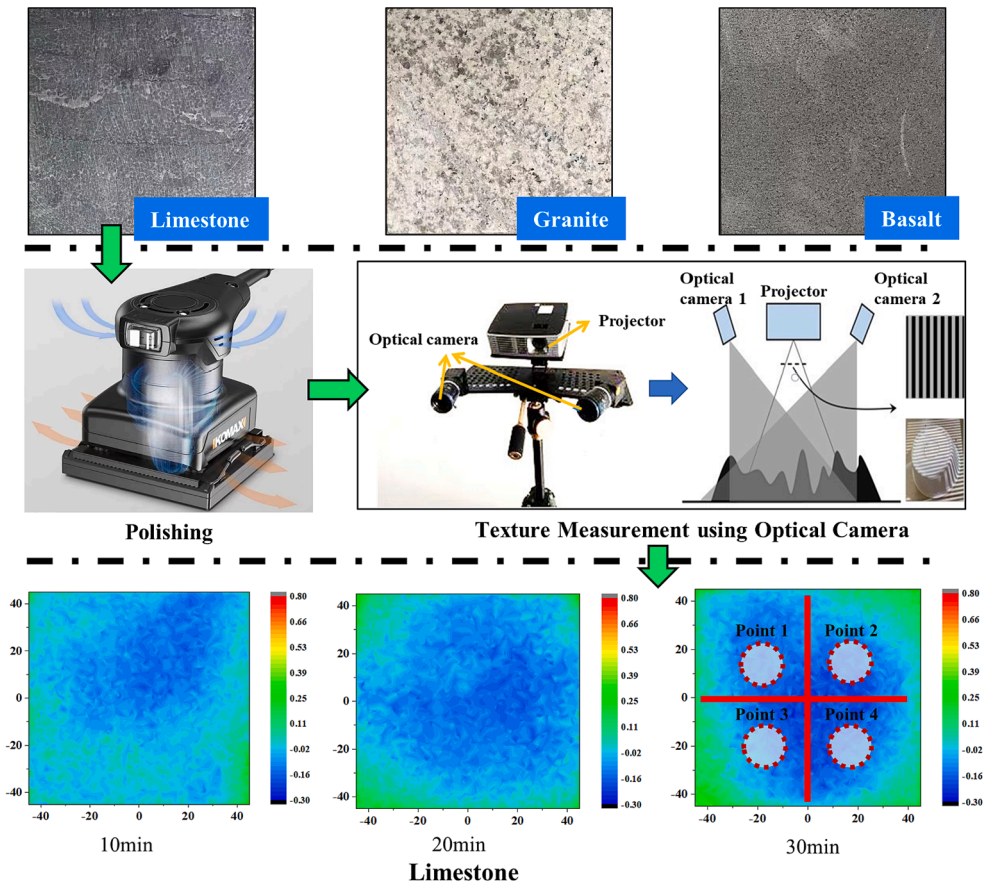

Fig. 1. The preparation of mineral surface with varying morphological characteristics.

Table 2
Polishing procedures used in this study.

Polishing type	Sandpaper type	Polishing time
Type 1	80 mesh	10 min
Type 2	80 mesh + 240 mesh	20 min
Type 3	80 mesh + 240 mesh + 320 mesh	30 min

Table 3
Combinations of samples and testing conditions in this study.

Bitumen	Unmodified bitumen
Mineral type	Basalt, Limestone, Granite
Polishing Type	Type 1, Type 2, and Type 3
Temperature	5 °C, 15 °C, and 25 °C,
Film thickness	10 μm–900 μm
Four repeated measures for each combination: 1080 times measurement in total	

the surface energy of mineral slabs can be accordingly obtained. In this study, the surface energies of the standard liquids are given in Table 5.

2.3.2. Characterization of bitumen-mineral interface failure

The pneumatic adhesion tensile tester was implemented to measure the bonding strength between bitumen and mineral surfaces. For the preparation of samples, a specific amount of bitumen related to a certain film thickness was weighed and heated to 150 °C and then dropped on the pull-off stub. Film thicknesses ranging from 10 μm to 900 μm with 100 μm intervals were taken into account as shown in Table 4. After that, the pull-off stub together with the bitumen and mineral slabs were put into a fully automated intelligent temperature incubator to maintain the measurement temperature for 30 min. Three measurement temperatures were considered, which were 5 °C, 15 °C, and 25 °C, respectively.

The whole procedure and measurement protocols can be referred to as standard [28]. After each measurement, the bonding strength between bitumen and mineral surfaces was recorded. In addition, failure images were collected through the camera for further analysis. Based on the digital image process (DIP), collected failure images were finally converted into binary images, in which the proportion of adhesive failure can be accordingly calculated by counting the white and black pixels, and vice versa for the proportion of cohesive failure.

3. Results and discussion

3.1. Morphological analysis of mineral surfaces

Fig. 5 presents the morphological characteristics of mineral surfaces with different polishing treatments concerning the mean texture depth and the adhesion energy. As the increase in polishing time, MTDs of the mineral surface increased linearly for different mineral types, which illustrated that the polishing treatment enhanced the roughness of mineral surfaces. The linear fitting results showed that the granite was the most sensitive to the polishing process, while the basalt and limestone presented an identical fitting slope. Herein, it was noticeable that the mineral surface was fabricated in the factory, which might show some difference from the natural surface of the aggregates. However, the focus of this study aimed to characterize the influence of the mineral surface on the adhesion/cohesion properties of the bitumen-mineral interface. Therefore, fabricating distinguished surface characteristics, to some extent, has achieved the goal in the scope of this study. The distribution of the scatters indicated some measurement deviations at a specific polishing time, which was on account of the non-uniformly polishing that occurred around the boundary of the mineral slab as

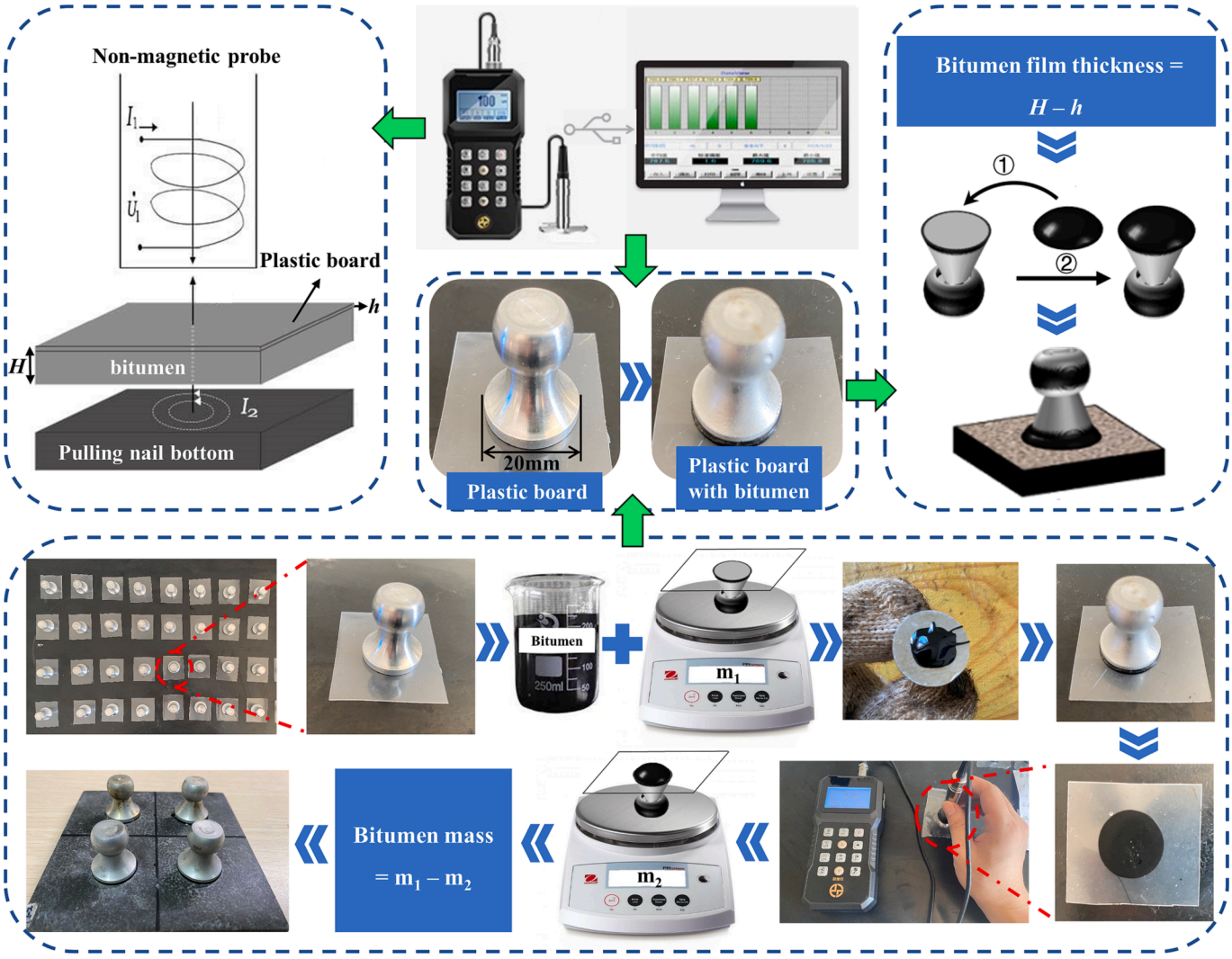

Fig. 2. Calibration of film thickness using thickness gauges.

Table 4
Bitumen mass used for the specific film thickness.

Thickness (μm)	10	100	200	300	400	500	600	700	800	900
Mass (g)	0.01	0.04	0.09	0.14	0.19	0.23	0.27	0.31	0.36	0.41

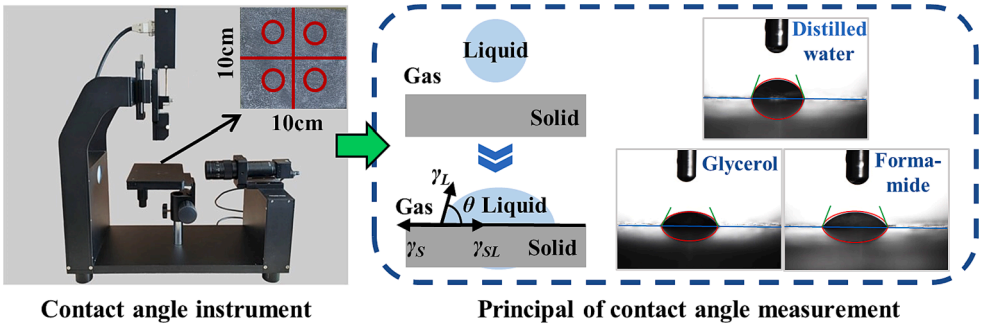

Fig. 3. Measurement of surface free energy for the mineral surfaces.

shown in Fig. 1.

The influence of polishing time on the calculated adhesion energy followed a similar tendency to that of MTD, as the adhesion energy of mineral surfaces increased linearly with the polishing time. On account of the contact angle measurement being limited in the middle area of the mineral slab, parallel measurements showed less variation in results.

Table 5
Surface energies of three reference liquids.

Reference liquids	Free energy parameter / (mJ/ m^2)		
	γ_l	γ_l^d	γ_l^p
Distilled water	72.8	21.8	51.0
Formamide	58.1	39.5	18.6
Glycerol	63.5	26.6	36.9

Fig. 6 presents the relationship between the MTD and the adhesion energy of mineral surfaces. It can be found that, in general, the MTD showed a positive relation to adhesive energy, as a higher MTD value induced a higher adhesion energy of mineral surfaces. This finding conformed to the previously reported conclusions in the literature and was also not difficult to understand. Although the coefficient of linear correlation was only 0.44 when all types of mineral surfaces were taken into account, the coefficient of linear correlation reached 0.87, 0.93, and 0.96 for basalt, granite, and limestone, respectively. Standing on this point, it was demonstrated that the mineral type significantly influenced the morphological characteristics of the mineral surface.

3.2. Influence of temperature and film thickness on the bonding strength

The analysis of variance (ANOVA) was performed on the measurement to identify whether the parameters would significantly influence the bond strength.

From Table 6, it can be observed that the P-values for film thickness, temperature, polishing time, and mineral type are all less than 0.05. This indicates that these four influencing factors have a significant impact on the bond strength of the bitumen-mineral interface.

Fig. 7 summarized the bonding strength measured at different mineral surfaces and varying measurement conditions. In terms of the influence of film thickness on the bonding strength. It can be concluded that, in general, the increase in the film thickness induced the reduction of bonding strength. A more specific tendency can be described as follows: when the film thickness increased starting from 10 μm, the bonding strength experienced a sharp decrease at the beginning stage. After that, the decreasing rate started to be slow until the bonding strength turned into a fluctuation stage.

Two additional conclusions should be compensated here. The sharp decreasing stage almost followed a linear reduction at the beginning stage. The other one was that there could exist two critical film thicknesses that depend on the mineral types and mineral morphology. The first critical film thickness was used to tell the linear decreasing stage and the later stages. The second critical film thickness referred to where the bonding strength would not change considerably as the continuing increase in the thickness. For example, the first critical film thickness that occurred for the basalt mineral with a 20 min polishing time was around 300 μm, however, it turned out to be 700 μm in the case of limestone with a 10 min polishing time. As for the second film thickness, it was observed in some cases of this study while some were not. As can be seen that the bonding strength of the granite mineral surface with the polishing time came to a plateau after 500 μm, particularly at the measuring temperature of 25 °C. However, the plateau did not appear for the limestone mineral surface with the polishing time of 20 min when the temperature was 5 °C or 15 °C.

On the other hand, the mineral type also played a crucial role in the bonding strength results even if following the same measurement condition. Regardless of the polishing time, the bonding strength for basalt and limestone showed comparable results, which in most cases were larger than the one measured for granite. This finding was consistent with existing recognition. The granite mineral is composed of acid mineral compositions, thus leading to a poor adhesion property with the bitumen. The maximum value of bonding strength from Fig. 7 occurred for the limestone mineral surface with the polishing time of 30 min, nevertheless, it was interesting to see that the lowest bonding strength was always recorded when the temperature was 25 °C, and more importantly with almost the same value around 1.5 MPa. It can be deduced that 1.5 MPa was the cohesive strength of bitumen. When the temperature was 25 °C, the failure mode was 100% cohesive failure, therefore, the measured bonding strength was independent of the mineral type and surface morphology. Nonetheless, the bonding strength was slightly increased at ultra-thin film thickness, which will be discussed in detail combined with the analysis of failure mode.

Concerning the influence of mineral morphology, it can be concluded that the change of mineral morphology would not cause significant variation in the bonding strength when the measuring temperature was 15 °C and 25 °C, respectively. However, when the measurement temperature was reduced to 5 °C, although with a comparable level of bonding strength, the decreasing tendency with the film thickness was altered to a great extent, especially for the granite mineral surface. This demonstrated that the influence of the micro-texture of the mineral surface would not significantly influence the bonding strength at a relatively high temperature. Besides, the mineral type behaved with a distinguished sensitivity to the change of mineral morphology at a relatively low temperature.

In the case of the limestone, the measured bonding strength at 5 °C was slightly inferior to the bonding strength at 15 °C. Although the stiffness of bitumen was influenced remarkably by the temperatures. The minor discrepancy indicated that the adhesive failure dominated the failure mode. In addition, it also demonstrated that the adhesion between bitumen and the mineral surface was better at a higher temperature. On the other hand, the extension of polishing time seems to contribute little to the variation of bonding strength between temperatures, again confirming the discussion on the above mineral morphology.

Compared with the limestone, the bonding strength between bitumen and basalt followed the contrast rule. In most cases, the

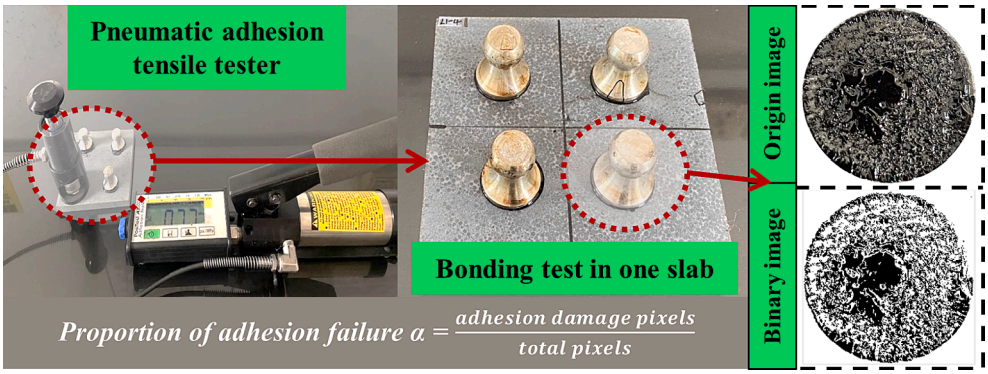

Fig. 4. Measurement of bonding strength around the bitumen-mineral interface.

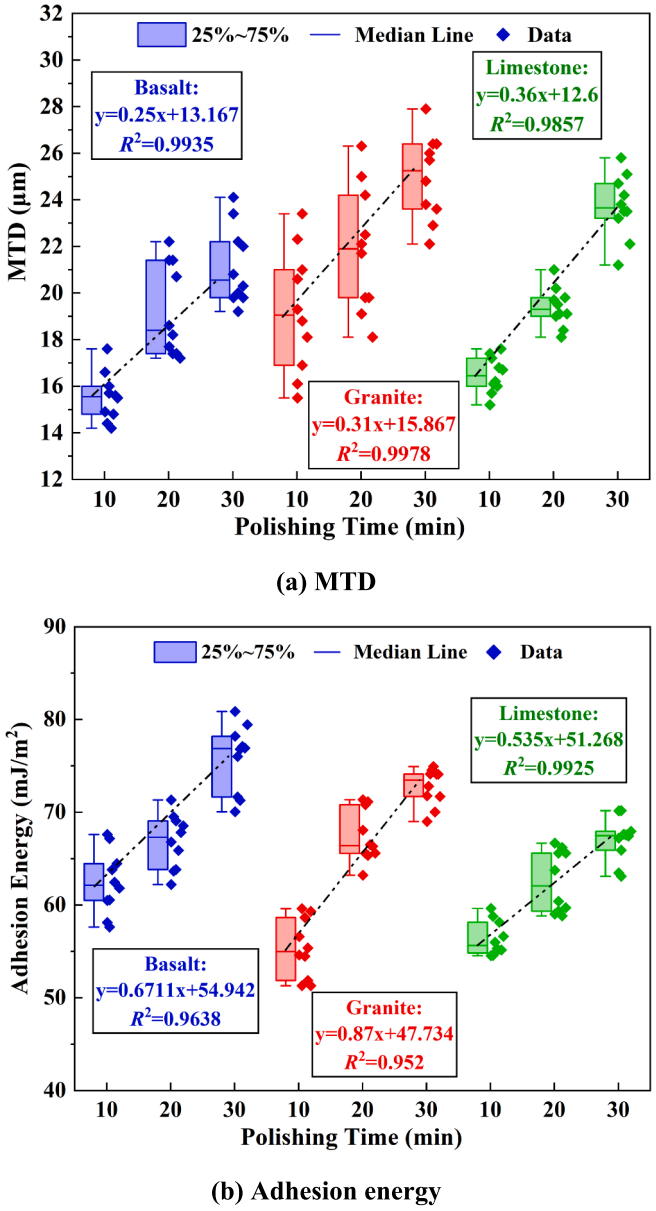

Fig. 5. Influence of polishing time on the mineral surface.

bonding strength measured at 5 °C was superior to that of 15 °C, claiming that the cohesive failure contributed to the interface failure. Some exclusions were also observed in the situation of a longer polishing time. Accordingly, it can be deduced that the increase in temperature (improving the adhesion property/weakening the cohesive strength) and the increase in surface roughness (also enhancing the adhesive strength) work together, consequently presenting a complicated tendency for different mineral types. Standing on this point, it can be concluded that, in the case of granite, the contribution of adhesion improvement exceeded that of cohesion weakening.

3.3. Adhesion/cohesion proportion around the bitumen-mineral interface

In the above section, the influence of temperature, surface morphology, mineral type, and film thickness on the bonding strength was comprehensively discussed. Nevertheless, a very critical influencing factor was not discussed, which was the proportion of cohesion and adhesion in one interface failure. However, the failure mode governed the bonding strength between the bitumen-mineral interface. The

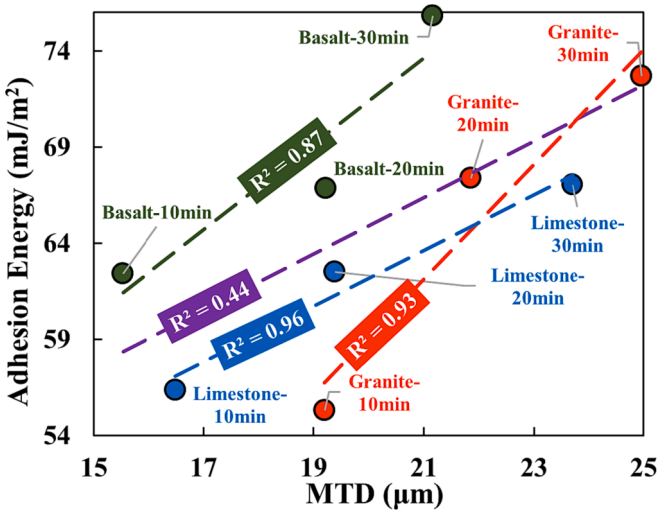

Fig. 6. Relationship between MTD and adhesion energy.

Table 6
ANOVA results for factors affecting bond strength.

Source	Sum of squares	df	Mean squares	F-value	P-value
Film thickness	78.277	9	8.697	59.676	<0.001
Temperature	58.936	2	29.468	202.190	<0.001
Polishing time	2.179	2	1.089	7.475	<0.001
Mineral type	6.891	2	3.446	23.642	<0.001

influence of film thickness on the bonding strength was associated with cohesive/adhesive failure, which will be discussed in this section.

Fig. 8 shows failure surface of the bitumen-mineral interface after bonding test in various situations. Since the influence of micro-texture on the bonding strength was not significant as concluded in the above section. Failure surface for the different polishing times were not presented and further discussed in this section. It can be observed that the influence of the measurement temperature and thickness on the cohesion/adhesion were both significant. In the case of the basalt at 15 °C, As the increase in the film thickness, the failure mode of the bitumen-mineral interface transferred from the cohesive/adhesive composite mode to the complete cohesive failure mode, which was in line with previously reported studies [11,29]. The identical rule can be seen in the situations of limestone and granite. So far, an extensively accepted mechanism for this phenomenon has not come to a consensus. Based on the experimental observation and analysis, a plausible explanation could be ascribed to the inhomogeneity essence caused by either the interfacial interaction that induces the re-ordering of the bitumen compositions or the inhomogeneity distribution of bitumen components once the observation scale reached a certain small level.

When the temperature increased to 25 °C, the failure mode was all cohesive failure mode even at an ultra-thin film thickness. The cohesive strength was considerably reduced on account of the temperature increase, as a result, the cohesive strength was remarkably smaller than the adhesive strength. Once the tensile loading was applied, the failure preferred to be damaged inside the bitumen binder, therefore performing a total cohesive failure mode. From this perspective, the ratio between cohesive and adhesive strength could be highly associated with the failure mode. If thinking one more step, it was not difficult to deduce that there exists a critical temperature where the complete cohesive failure mode started to occur. Given a total cohesive failure, another interesting phenomenon can be observed as highlighted by the green rings. Almost all cohesive failure images were presented in the form of the lunar crater and as the film thickness increased, the diameter of the lunar crater increased progressively. This indirectly demonstrated the

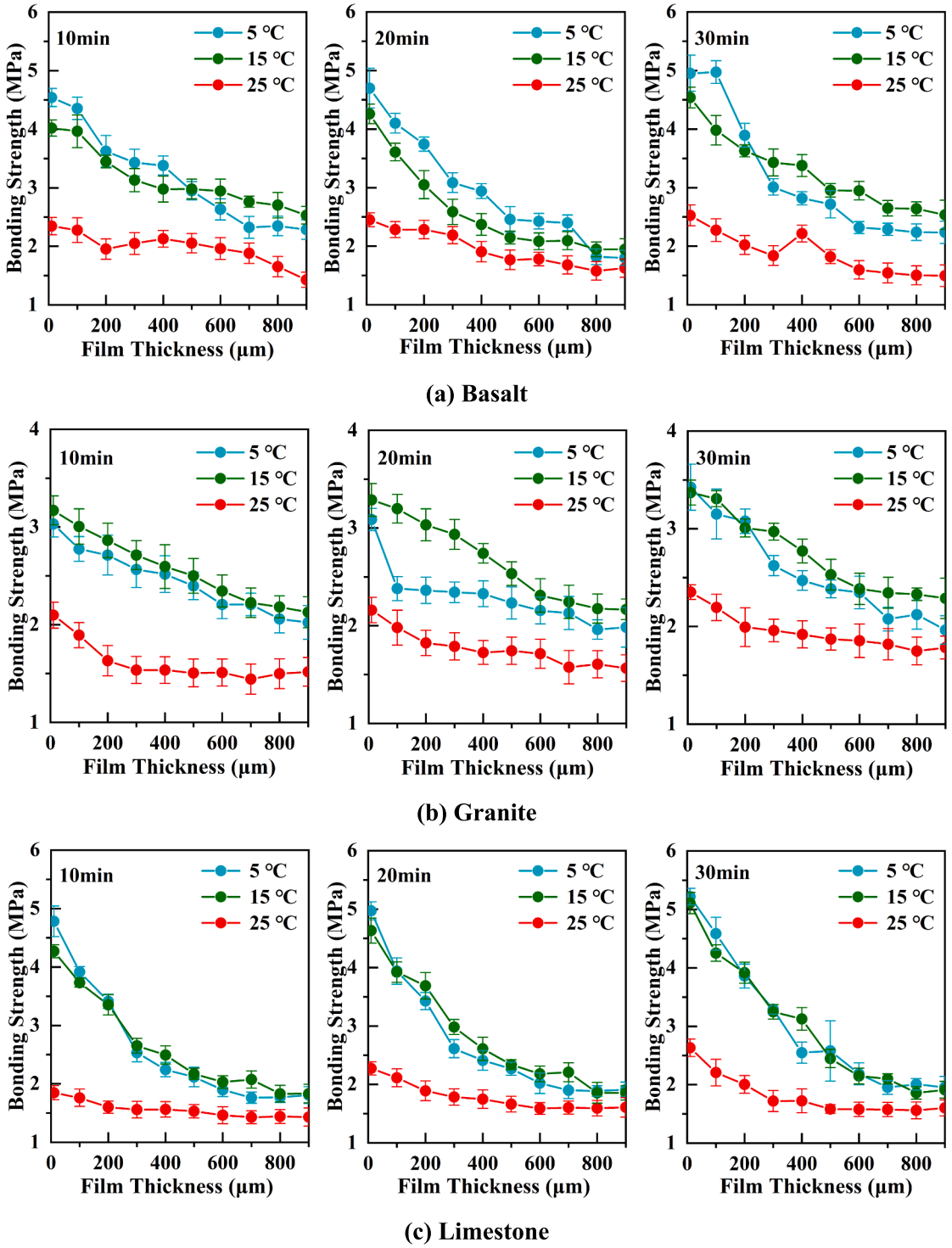

Fig. 7. Influence of film thickness on bonding strength.

inhomogeneity essence of the bitumen. When the film thick decreased, the scale effect progressively increased, thus leading to a denser distribution of lunar craters.

Figs. 9 and 10 show calculated proportions of adhesion changed with the film thickness, following the equation shown in Fig. 4. As Fig. 8 indicated that when the temperature was set at 25 °C, the failure mode was transferred into the cohesive failure. Therefore, the proportion of adhesion was not calculated for the analysis.

As the increase of film thickness, the proportion of adhesion showed the same tendency as the bonding strength. On the other hand, the reduction of adhesion proportion could be the reason for the decrease in bonding strength. This finding enlightened that the essential adhesive property was not changed with the film thickness. The variation in measured bonding strength was attributed to the variation in the cohesive/adhesive failure mode. Comparing the proportion of adhesion for three types of mineral surfaces, it can be concluded that the value increased following the sequence of basalt, granite, and limestone. Although many theories have been proposed to explain the influence of mineral type on the adhesive properties between bitumen and aggregates. The preference for adhesive failure mode around the bitumen-

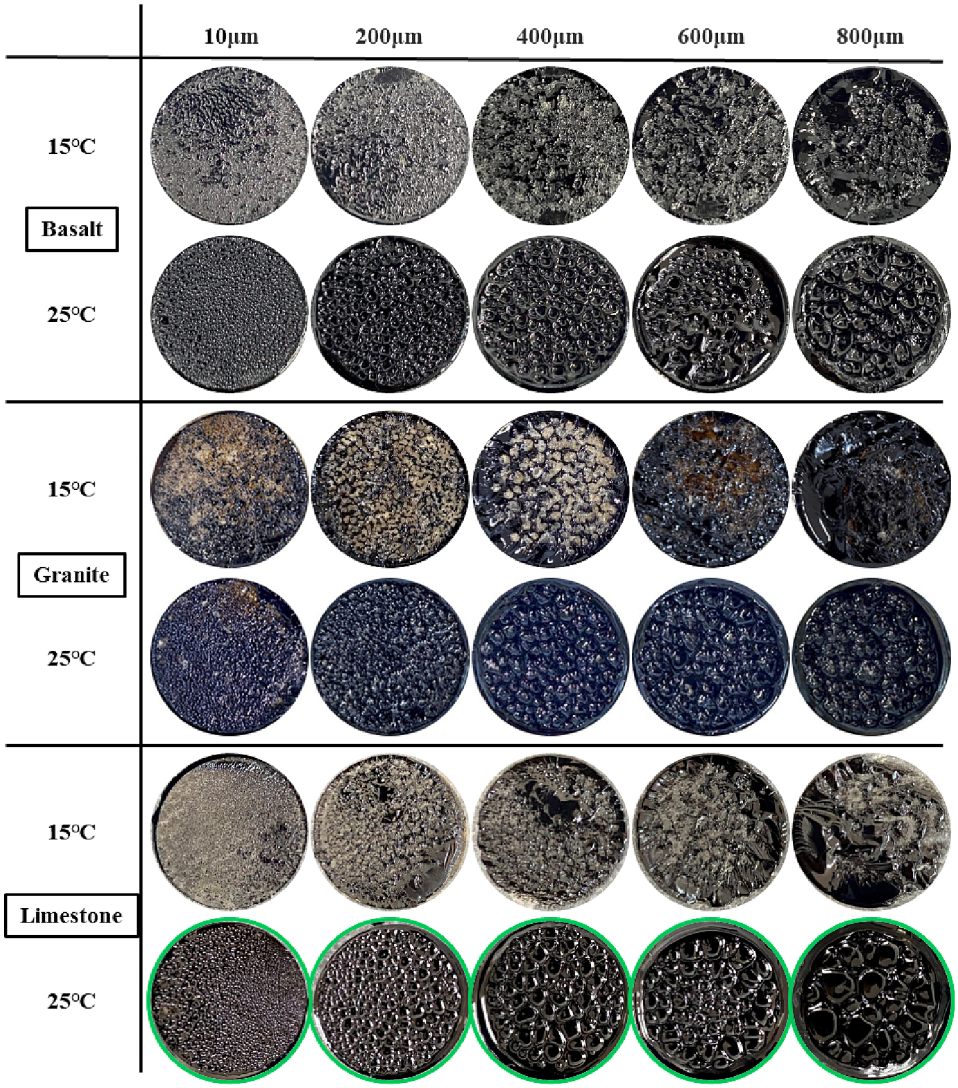

Fig. 8. Failure surface of the bitumen-mineral interface after the bonding test.

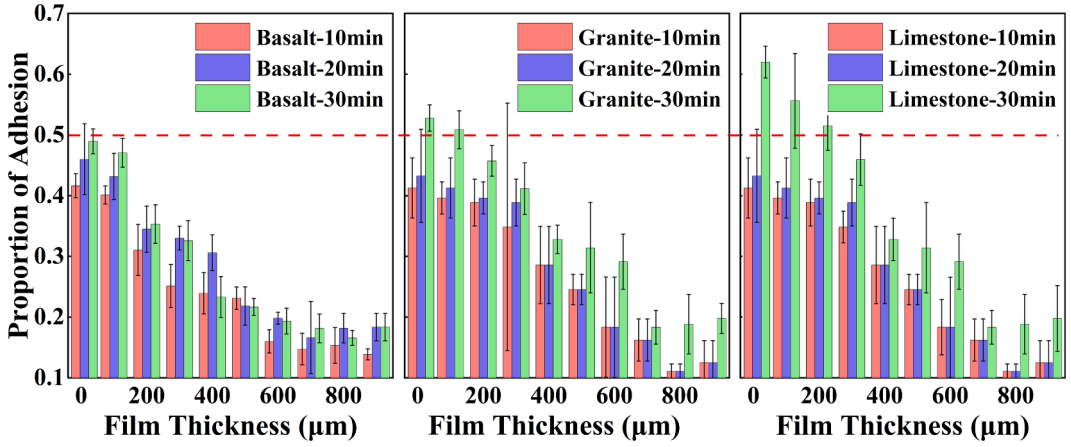

Fig. 9. Proportion of adhesive failure after bonding test at 5 °C.

mineral interface could be a previously ignored mechanism.

With the increase in polishing time, the proportion of adhesion increased for all cases, which indicated that the micro-texture also contributed to the proportion of adhesive failure. In specific, it can be described as the increase in MTD induced a high proportion of adhesive failure mode, which was favorable for the bonding strength between bitumen and minerals. Comparing the temperature 5 °C and 15 °C, the critical value 0.5 was marked as the red dot line to tell which kind of

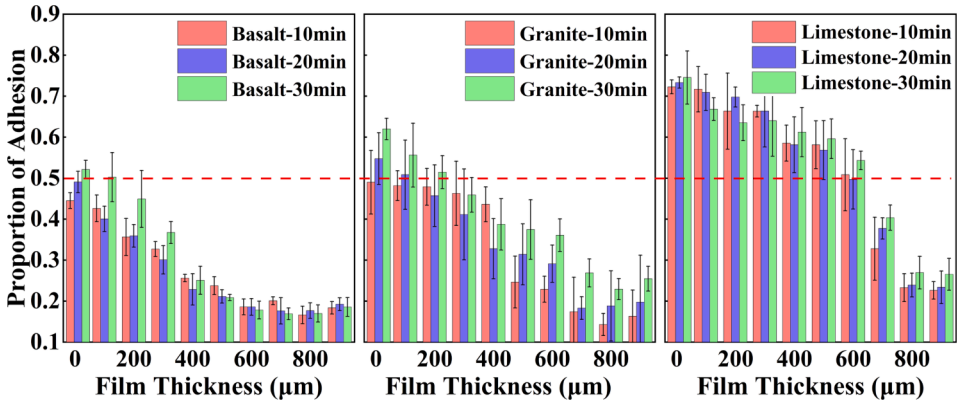

Fig. 10. Proportion of adhesive failure after bonding test at 15 °C.

failure mode dominated. In most cases when the temperature was 5 °C, the cohesion dominated the failure mode. However, when the temperature increased to 15 °C, particularly for the limestone, the adhesion dominated the failure mode.

4. Conclusions

This study focused on the failure mode around the bitumen-mineral interface. To this end, the influence of film thickness, micro-textures, temperature, and mineral type on the interfacial failure in terms of the bonding strength and failure modes were considered and comprehensively discussed. Major findings were summarized as follows:

(1) The MTD and adhesion energy showed a good correlation with each other. By polishing the mineral surfaces, the variation of MTDs and adhesion energy can be effectively created.
(2) With the increase of film thickness, the bonding strength decreased progressively and until reaching a critical film thickness, the bonding strength was almost unchanged, indicating that the cohesion damage dominated the interface failure mode. In addition, the proportion of adhesion progressively decreased with the increase in film thickness at 5 °C and 15 °C. When the temperature reached 25 °C, the interface failure was a complete cohesive failure.
(3) Concerning the cohesive failure, the failure surface was observed with the lunar craters, demonstrating the inhomogeneity of bitumen components. The scale effect of film thickness cannot be ignored, which determined when the bitumen should be regarded as homogeneous or not.

It is important to emphasize that the failure mechanism at the bitumen-aggregate interface is much more complex. Therefore, further studies should focus on quantitative analysis of the hybrid failure mode. Based on the above findings, future research can be conducted from a multi-scale perspective, such as exploring the influence of wetting conditions, developing empirical and mechanical models of the hybrid failure, to compensate for the limitations of this study.

CRediT authorship contribution statement

Baocun Shi: Writing – original draft, Visualization, Software, Investigation, Formal analysis, Data curation. **Quan Liu:** Writing – review & editing, Supervision, Methodology, Conceptualization. **Yangming Gao:** Methodology, Conceptualization. **Jiantao Wu:** Project administration, Conceptualization. **Jingya Chen:** Supervision.

Declaration of Competing Interest

The authors declare that they have no known competing financial interests or personal relationships that could have appeared to influence the work reported in this paper.

Data availability

Data will be made available on request.

Acknowledgments

The authors would like to acknowledge the financial support provided by the Natural Science Youth Fund of Jiangsu Province (No. BK20220983), the Excellent Master's Degree Thesis Cultivation Project of Hohai University (No. 422003512), the National Science Foundation of China (No. 52078190), and the Natural Science Foundation of Jiangsu Province (No. BK20221501).

References

[1] K. Kanitpong, H. Bahia, Relating adhesion and cohesion of asphalts to the effect of moisture on laboratory performance of asphalt mixtures, Transp. Res. Rec.: J. Transp. Res. Board. 2005 (1901) 33–43, https://doi.org/10.1177/0361198105190100105.
[2] P. Chaturabong, H.U. Bahia, Effect of moisture on the cohesion of asphalt mastics and bonding with surface of aggregates, Road Mater. Pavement Des. 19 (2018) 741–753, https://doi.org/10.1080/14680629.2016.1267659.
[3] D.E. Packham (Ed.), Handbook of Adhesion, Wiley, 2005.
[4] E. Masad, L. Tashman, D. Little, H. Zbib, Viscoplastic modeling of asphalt mixes with the effects of anisotropy, damage and aggregate characteristics, Mech. Mater. 37 (2005) 1242–1256, https://doi.org/10.1016/j.mechmat.2005.06.003.
[5] A.W. Hefer, D.N. Little, R.L. Lytton, I.L. Al-Qadi, M. Taylor, G. King, D. Anderson, A synthesis of theories and mechanisms of bitumen-aggregate adhesion including recent advances in quantifying the effects of water, Asphalt Paving Technology: Association of Asphalt Paving Technologists-Proceedings of the Technical Sessions. 74 (2005) 139–195.
[6] S.C. Huang, J.F. Branthaver, R.E. Robertson, Interaction of asphalt films with aggregate surfaces in the presence of water, Road Mater. Pavement Des. 3 (2002) 23–48, https://doi.org/10.1080/14680629.2002.9689914.
[7] A. Bhasin, Development of methods to quantify bitumen-aggregate adhesion and loss of adhesion due to water, Texas A&M University, 2007.
[8] H. Wang, J. Wang, J. Chen, Micromechanical analysis of asphalt mixture fracture with adhesive and cohesive failure, Eng. Fract. Mech. 132 (2014) 104–119, https://doi.org/10.1016/j.engfracmech.2014.10.029.
[9] J. Hu, Z. Qian, The prediction of adhesive failure between aggregates and asphalt mastic based on aggregate features, Constr. Build. Mater. 183 (2018) 22–31.
[10] C. Li, Q. Liu, J. Lei, Z. Zhang, C. Fu, F. Pan, Influence of mineral fillers properties on the bonding properties of bitumen mastics, Constr. Build. Mater. 318 (2022), 126013, https://doi.org/10.1016/j.conbuildmat.2021.126013.
[11] V. Mishra, D. Singh, Evaluating factors affecting aggregate-bitumen interfacial strength using binder bond-strength test, J. Mater. Civ. Eng. 33 (2021) 1–13, https://doi.org/10.1061/(asce)mt.1943-5533.0003703.
[12] G. Huang, J. Zhang, Z. Wang, F. Guo, Y. Li, L. Wang, Y. He, Z. Xu, X. Huang, Evaluation of asphalt-aggregate adhesive property and its correlation with the interaction behavior, Constr. Build. Mater. 374 (2023), 130909, https://doi.org/10.1016/j.conbuildmat.2023.130909.

[13] M. Arbabpour Bidgoli, P. Hajikarimi, M.R. Pourebrahimi, K. Naderi, A. Golroo, F. Moghadas Nejad, Introducing adhesion-cohesion index to evaluate moisture susceptibility of asphalt mixtures using a registration image-processing method, J. Mater. Civ. Eng. 32 (2020), https://doi.org/10.1061/(asce)mt.1943-5533.0003477.
[14] Y. Lu, L. Wang, Nanoscale modelling of mechanical properties of asphalt-aggregate interface under tensile loading, Int. J. Pavement Eng. 11 (2010) 393–401, https://doi.org/10.1080/10298436.2010.488733.
[15] Y. Gao, Y. Zhang, F. Gu, T. Xu, H. Wang, Impact of minerals and water on bitumen-mineral adhesion and debonding behaviours using molecular dynamics simulations, Constr. Build. Mater. 171 (2018) 214–222, https://doi.org/10.1016/j.conbuildmat.2018.03.136.
[16] Y. Gao, Y. Zhang, Y. Yang, J. Zhang, F. Gu, Molecular dynamics investigation of interfacial adhesion between oxidised bitumen and mineral surfaces, Appl. Surf. Sci. 479 (2019) 449–462, https://doi.org/10.1016/j.apsusc.2019.02.121.
[17] P. Chen, X. Luo, Y. Gao, Y. Zhang, Modeling percentages of cohesive and adhesive debonding in bitumen-aggregate interfaces using molecular dynamics approaches, Appl. Surf. Sci. 571 (2022), 151318, https://doi.org/10.1016/j.apsusc.2021.151318.
[18] A. Cala, S. Caro, M. Lleras, Y. Rojas-Agramonte, Impact of the chemical composition of aggregates on the adhesion quality and durability of asphalt-aggregate systems, Constr. Build. Mater. 216 (2019) 661–672, https://doi.org/10.1016/j.conbuildmat.2019.05.030.
[19] A. Cala, S. Caro, Predictive quantitative model for assessing the asphalt-aggregate adhesion quality based on aggregate chemistry, Road Materials and Pavement Design. 23 (2022) 1523–1543, https://doi.org/10.1080/14680629.2021.1900896.
[20] J.E. Howson, Relationship between surface free energy and total work of fracture of asphalt binder and asphalt binder-aggregate interfaces, 2011.
[21] J. Zhang, A.K. Apeagyei, G.D. Airey, J.R.A. Grenfell, Influence of aggregate mineralogical composition on water resistance of aggregate-bitumen adhesion, Int. J. Adhes. Adhes. 62 (2015) 45–54, https://doi.org/10.1016/j.ijadhadh.2015.06.012.
[22] F. Canestrari, F. Cardone, A. Graziani, F.A. Santagata, H.U. Bahia, Adhesive and cohesive properties of asphalt-aggregate systems subjected to moisture damage, Road Mater. Pavement Des. 11 (2010) 11–32, https://doi.org/10.1080/14680629.2010.9690325.
[23] Ministry of Transport of the People's Republic of China, Standard test methods of bitumen and bituminous mixtures for highway engineering (JTG E20-2011), (2011).
[24] H. Wang, J. Ma, H. Yang, F. Sun, Y.a. Wei, L. Wang, Development of three-dimensional pavement texture measurement technique using surface structured light projection, Meas.: J. Int. Meas. Confederation. 185 (2021), 110003, https://doi.org/10.1016/j.measurement.2021.110003.
[25] D. Singh, V. Mishra, Different methods of selecting probe liquids to measure the surface free energy of asphalt binders, Constr. Build. Mater. 175 (2018) 448–457, https://doi.org/10.1016/j.conbuildmat.2018.04.199.
[26] V. Mishra, D. Singh, A. Habal, Investigating the condition number approach to select probe liquids for evaluating surface free energy of bitumen, Int. J. Pavement Res. Technol. 13 (2020) 10–19, https://doi.org/10.1007/s42947-019-0097-x.
[27] Z. Fan, C. Du, P. Liu, D. Wang, M. Oeser, Study on interfacial debonding between bitumen and aggregate based on micromechanical damage model, Int. J. Pavement Eng. 23 (2022) 340–348, https://doi.org/10.1080/10298436.2020.1745800.
[28] D. ASTM, Standard test method for pull-off strength of coatings using portable adhesion testers, ASTM International: West Conshohocken, PA, USA, 2017.
[29] R. Bionghi, D. Shahraki, M. Ameri, M.M. Karimi, Correlation between bond strength and surface free energy parameters of asphalt binder-aggregate system, Constr. Build. Mater. 303 (2021), 124487, https://doi.org/10.1016/j.conbuildmat.2021.124487.